On the robustness of the r-process in neutron-star mergers

Joel de Jesús Mendoza-Temis,[1] G. Martínez-Pinedo,[1,2] K. Langanke,[2,1,3] A. Bauswein,[4] and H.-T. Janka[5]

[1] *Institut für Kernphysik (Theoriezentrum), Technische Universität Darmstadt, Schlossgartenstraße 2, 64289 Darmstadt, Germany*
[2] *GSI Helmholtzzentrum für Schwerionenforschung, Planckstraße 1, 64291 Darmstadt, Germany*
[3] *Frankfurt Institute for Advanced Studies, Ruth Moufang Str. 1, D-60438 Frankfurt, Germany*
[4] *Department of Physics, Aristotle University of Thessaloniki, 54124 Thessaloniki, Greece*
[5] *Max-Planck-Institut für Astrophysik, Postfach 1317, 85741 Garching, Germany*

We have performed r-process simulations for a set of trajectories describing matter ejected in neutron star mergers. Our calculations consider an extended nuclear network, including spontaneous, β- and neutron-induced fission and adopting fission yield distributions from the ABLA code. In particular we have studied the sensitivity of the r-process abundances on the nuclear mass models by using different models. We find that the general features of the observed r-process abundance distribution (the second and third peaks, the rare-earth peak and the lead peak) are reproduced by our simulations, independently of the merger trajectory, and for all mass models. We find distinct differences in the predictions of the mass models at and just above the third peak, which can be traced back to different predictions of neutron separation energies for r-process nuclei around neutron number $N = 130$. In all simulations, we find that the second peak around $A \sim 130$ is produced by the fission yields of the material that piles up in nuclei with $A \gtrsim 250$ due to the substantially longer beta-decay half-lives found in this region. The third peak around $A \sim 195$ is generated in a competition between neutron captures and β decays during r-process freeze-out. We find that at timescales of weeks relevant for kilonova light curve calculations, the abundance of actinides is larger than the one of lanthanides. This means that actinides can be even more important than lanthanides to determine the photon opacities under kilonova conditions.

PACS numbers: 26.30.Hj, 26.50.+x, 97.60.Jd

I. INTRODUCTION

The astrophysical r-process produces about half of the heavy elements in the Universe, including all of the actinides [1, 2]. It is commonly accepted that it occurs as a sequence of neutron captures and β decays in environments with extreme neutron densities. Under such conditions neutron captures are much faster than β decays and the r-process path runs through nuclei with large neutron excess far off stability [3, 4].

The actual astrophysical site of the r-process is yet not known. For many years the neutrino-driven wind from the surface of a freshly born neutron star in a core-collapse supernova has been the favored site [5]. However, recent supernova simulations with improved nuclear input, realistic neutrino transport and advanced multi-dimensional treatment of hydrodynamics [6] indicate that the conditions of the matter ejected in the wind (entropy, expansion velocity, proton-to-neutron ratio) are not suited to support an r-process which produces the elements in the third peak (around mass number $A \sim 195$) and beyond. However, the neutrino-driven wind might significantly contribute to the abundance of the lighter elements up to the second peak ($A \sim 130$) [7–9]. The shortfall of the neutrino-driven wind model to produce the heavier r-process elements has revived the interest in another potential site, the merger of two neutron stars (NS merger) [10, 11].

Simulations of NS mergers indicate that the matter ejected during the dynamical phase is very neutron rich with extremely large neutron-to-seed ratios ($R_{n/s} > 500$) [12–14]; i.e. there are many neutrons which can be captured by seed nuclei transporting matter to very heavy nuclei in the region of the nuclear chart where decay by fission is possible. The intermediate-mass fission yields are then subject to neutron captures establishing the occurrence of a few fission cycles, which are expected to produce the heavier r-process elements in a rather robust way with nearly relative solar abundances. We note that such a robust scenario is quite attractive as it might explain the occurrence of r-process elements above the second peak in solar proportion as observed in very old metal-poor stars [15]. An additional source of ejected material with relevance for r-process nucleosynthesis comes from the accretion disk formed around the compact object resulting from the merger. However, the conditions in these ejecta are more sensitive to the details of the astrophysical parameters and microphysics included [16–19]. Here we will consider only the initial dynamical ejecta.

To serve as the site for the production of heavy r-process elements and to explain the observation of the elemental abundances in solar proportion in metal-poor stars, the r-process in NS mergers should not depend on particular astrophysical conditions, e.g. on the specific combination of NS masses in the merging binary system. It is unsatisfactory for r-process abundance simulations that most nuclei encountered during the process have yet not been produced in the laboratory and hence their properties depend on nuclear models and are yet quite uncertain.

The sensitivity of r-process nucleosynthesis in dynamical ejecta of NS mergers to the astrophysical conditions, i.e. neutron star masses, orbit parameters, has been studied in [12–14]. Korobkin *et al.* have performed r-process simulations for a set of NS mergers consisting of various combinations of neutron stars in the relevant mass range between 1 and 2 $M_\odot$ [13], while Bauswein *et al.* have explored the influence of various equations of state on the merger dynamics and nucleosynthesis [14]. It turns out that the specific treatment of the merger dynamics, e.g. Newtonian vs General Relativistic mechanics, leads to fundamentally different mass ejection dynamics [13, 14]. Importantly for our discussion both groups find, within their treatment, nearly identical abundance distributions between the second and third peaks for all of the 23 combinations of neutron stars [13] or the various adopted equations of state [14], pointing to virtually no sensitivity of the relative abundance of heavy elements on the astrophysical conditions of the mergers. However, both groups also found strong sensitivity of the abundances to the treatment of fission. Indeed, the calculations of [13] show an abundance hole around $A \sim 140$, relative to solar, while in the study of Ref. [14] the second peak is noticeably shifted to larger mass numbers. Both effects are related to the treatment of fission adopted in the respective simulations.

This dependence on fission as well as the effect of half lives and neutron separation energies (masses) on the r-process abundances in NS merger simulations has been the focus of three simultaneous and independent studies. Eichler *et al.* have confirmed the strong sensitivity on the fission yield distribution [20]. However, they succeeded to show that fission yields derived with the ablation-abrasion model code ABLA [21, 22], which is based on the statistical model, cured the shortcomings in the abundance distribution above the second peak. The ABLA code is adjusted to reproduce fission data and considers the evaporation of free neutrons before and after the fission process. However, these neutrons as well as those which are produced by beta-delayed neutron emission of the fission fragments can be captured by nuclei after freeze-out resulting in a slight shift of the third peak to heavier mass numbers than is observed in the solar abundances. Eichler *et al.* argue that such a shift can be avoided by faster β decays than those predicted by the Finite Range Droplet Model (FRDM) model which has been adopted in their study. In an independent study Caballero *et al.* come to the same conclusion [23] when they compare results of NS merger r-process simulations performed with the half lives based on the FRDM model with those obtained by replacing these half lives with faster values derived by QRPA calculations on top of the DF energy functional of Fayans [24]. Importantly, these faster DF-based half lives agree well with recent experimental data obtained for nuclei close and on the r-process path, including data for neutron-rich nuclei towards the $N = 126$ waiting points [25]. Here, the DF-based half-lives, in close agreement with recent large-scale shell model calculations [26, 27], point to the importance of forbidden transitions to the β decays.

In this manuscript, we study the effect of nuclear masses and neutron capture rates on the r-process in NS mergers. Masses are particularly important as they, via the neutron separation energies, define the r-process path in the nuclear chart and secondly they are crucial ingredients in the statistical model calculation of neutron capture cross sections. In the following we will derive neutron separation energies as well as neutron capture cross sections consistently from the same mass models. Furthermore photodissociation cross sections are obtained by detailed balance from the capture cross sections. As the masses of the extremely neutron-rich nuclei on the r-process path are not known experimentally, they have to be modeled. For many years, masses derived on the basis of the Finite Range Droplet Model (FRDM) [28] and the ETFSI model (Extended Thomas Fermi Model with Strutinski Integral,[29]) have been a standard in r-process simulations. Recently Wang and Liu developed an alternative microscopic-macroscopic mass model (Weizsäcker-Skyrme or WS3 model [30]), which employs a Skyrme energy density formula as a macroscopic basis, which is then microscopically supplemented by shell corrections. Guided by intuition derived from the interacting shell model, Duflo and Zuker developed a mass formula based on a systematic description of occupation numbers and taking special care of the role of intruder states [31]. There exists two versions of the Duflo-Zuker mass formula on the market: one with 31 parameters (called DZ31) and one with 10 parameters (DZ10). Finally advances in computing resources make it now possible to derive mass formulas on the basis of microscopic nuclear many-body models, like the Hartree-Fock-Bogoliubov (HFB) model. In a sequence of continuous improvements of the Skyrme functional, which is the basis of their model, Goriely and collaborators have succeeded to obtain an HFB mass model which is comparative to the phenomenological models, like FRDM and ETFSI, and can be globally applied in r-process simulations [32]. In the following we will use the model HFB21 [33].

To explore the sensitivity of the r-process in NS mergers on the nuclear masses, we have performed a set of r-process simulations using identical astrophysical conditions, which we take from a 3-dimensional relativistic simulation of the merger of two neutron stars with 1.35 $M_\odot$, which is expected to be the most frequent NS merger system. We use five different mass models (FRDM, WS3, DZ10, DZ31, HFB21) for the calculation of neutron capture rates that enter in the r-process simulations. Overall our calculations yield 'robust' r-process abundance patterns reaching from the second r-process peak up to the actinides, with modest but interesting and distinct differences between the various models and an overall satisfying agreement with the solar r-process abundances.

Our paper is organized as follows. In the next section

we give a brief description of our r-process simulations and the input being used. The results of our simulations for the r-process abundances and their dependence on the adopted mass models are presented and discussed in section III. Finally, we conclude in section IV.

II. NS MERGER TRAJECTORIES AND NUCLEAR INPUT

The r-process calculations in this work are based on fluid element trajectories that were extracted from hydrodynamical simulations of NS mergers to represent the conditions of matter becoming unbound from such events. The merger simulations were performed with a 3-dimensional relativistic smoothed particle hydrodynamics code [14, 34–36], which imposes conformal flatness on the spatial 3-metric to solve the Einstein equations in an approximate manner [37, 38]. The calculations started from initial data representing close binary systems in quasi-equilibrium a few orbits before merging. Initially the NS matter was in neutrino-less beta-equilibrium at zero temperature. The initial electron fraction was advected with the fluid during the hydrodynamical simulations without taking into account neutrino processes. This simplification was a reasonably good approximation in Newtonian models (e.g. [39]), but the impact of neutrinos in relativistic merger models requires further investigation [40]. NS matter is modelled with the TM1 EoS [41–43], which leads to a NS radius of 14.49 km for a 1.35 $M_\odot$ NS and a maximum gravitational mass of 2.21 $M_\odot$ for nonrotating NSs.

In this work we focused on a binary system of two NSs with gravitational masses of 1.35 $M_\odot$, which may be representative for the observed double NS systems (see e.g. [44] for a compilation of measured binary NS masses). In the simulation we found most unbound matter originating from the contact interface during the coalescence (see [14] for a detailed description of the merger dynamics and ejection mechanism). Originating from the inner NS crust these ejecta are very neutron-rich. The time-step limitations of the NS simulations allowed to follow the ejecta only for several 10 milliseconds. Hence, we have analytically continued the trajectories to later times than considered in the simulations by evolving the density assuming a power law, i.e. $\rho(t) = \rho(t_0)\left(\frac{t_0}{t}\right)^n$. In our calculations we have used $n = 2$ and $n = 3$, without noticeable differences in the abundance results. In the following we will adopt $n = 2$.

For our r-process simulations we have picked a set of trajectories which cover the range of electron-to-nucleon ratios, Y_e, and expansion timescales representative of the ejected matter in the NS merger calculation of Ref. [14]. We have started our r-process calculations at densities around $\rho = 4 \times 10^{11}$ g cm^{-3} as at higher densities β decays are Pauli blocked due to the high Fermi energy of electrons in the dense medium. The initial matter composition, appropriate for the different trajectories at this density, has been determined assuming that matter is in Nuclear Statistical Equilibrium (NSE) at the sufficiently high temperatures involved. While the details of the initial composition depend on the conditions of the trajectories and on the mass models used, we can generally observe that they are given by neutron-rich nuclei centered around magic neutron numbers $N = 50$ and $N = 82$, while proton numbers in the iron-nickel range are favored in the first case and around strontium-zirconium in the second. The relative weight of these two composition peaks depends on entropy, favoring the peak around mass number $A \sim 120$ relative to the one around $A \sim 80$ with decreasing entropy.

Starting from these initial compositions we have followed the r-process evolution by a large network. The dynamics of the process was governed by the astrophysical trajectories, however, consistently corrected for reheating by energy release in nuclear reactions, as we describe below. Our network includes more than 7300 nuclei which cover the nuclear chart from free nucleons up to ^{313}Ds. As nuclear reactions among these nuclei we considered charge particle reactions, neutron captures and its inverse process, photo-dissociation, and β and α decay and fission. We have derived the neutron capture rates consistently for each individual mass model within the statistical model using the code MOD-Smoker [45]. The photodissociation rates were obtained from the neutron capture rates by detailed balance. For nuclei, for which the half lives are not known experimentally, we have adopted the β decay (and β delayed neutron emission) rates from the compilation of Möller *et al.* [46], which was derived from QRPA calculations on top of the FRDM mass model. We used the parametrization of Ref. [47] of the Viola-Seaborg formula to estimate the α-decay rates, which become relevant for heavy nuclei beyond lead. Finally, for fission reactions we included contributions from neutron-induced fission taken from [48] that are based on the FRDM mass model [28] and the Thomas-Fermi barriers of Myers and Swiatecki [49]. Rates for β delayed and spontaneous fission were adopted from [50]. Our fission yields were taken from the calculations of Ref. [51] which were derived using the code ABLA. This approach also gives a consistent estimate for the number of neutrons set free during the fission process.

Nuclear reactions change the energy balance of the environment. We take this into account following refs. [11] by calculating, at any time of the evolution, the change in abundances in the various nuclei by solving the nuclear network. The related energy release is mainly connected to β decays where we assume that half of the energy set free in the process is carried away by the neutrino [52, 53]. In the next step, the energy release can be translated into a change of entropy, from which we calculated a new temperature using the equation of state of Ref. [54] which considers nucleons, nuclei, electrons, positrons and photons.

III. RESULTS

A. Time evolution and energy generation

We have started our r-process simulations for the various trajectories at densities $\rho = 4 \times 10^{11}$ g/cm^3 assuming an initial NSE composition. As a striking feature, we note the very large neutron-to-seed ratios ($R_{n/s} \approx 600 - 2000$) which is a prerequisite of r-process nucleosynthesis for nuclides beyond the third peak reaching the region in the nuclear chart where nuclei decay by fission. Furthermore, due to the extremely high neutron densities involved, the path of the r-process in NS mergers runs through nuclei close to the dripline. For these nuclei, with their large Q values, β decays are fast (order ms or faster).

Before we study the nucleosynthesis results of our simulations we like to make some important remarks concerning the heating of the astrophysical medium by nuclear reactions, mainly by β decays. In Fig. 1 we show the evolution of density, temperature and the energy release due to nuclear reactions for the selected trajectories and the different mass models considered. The evolution using the DZ10 mass model is very similar to DZ31 and not shown. We note that there is a noticeable spread among the trajectories. However, the temperature evolution shows quite similar pattern for the different mass models and trajectories. Its behavior can be understood from basic thermodynamics. From the first law of thermodynamics the energy per nucleon released by nuclear reactions, $\dot{q}$, is related to the change of the energy per nucleon, ε and nucleon density, $n = \rho/m_u$ (m_u the atomic mass unit), as:

$$\dot{q} = \frac{d\varepsilon}{dt} - \frac{P}{n^2}\frac{dn}{dt} = c_V \frac{dT}{dt} + \left(\frac{d\varepsilon}{dn} - \frac{P}{n^2}\right)\frac{dn}{dt}. \quad (1)$$

where $c_V = d\varepsilon/dT$ is the specific heat per nucleon at constant volume. The evolution of temperature reduces to:

$$\frac{dT}{dt} = \frac{1}{c_V}\left[\dot{q} - \frac{1}{\tau_n}\left(\frac{P}{n} - n\frac{d\varepsilon}{dn}\right)\right] \quad (2)$$

where we have introduced the expansion timescale $1/\tau_n = -(dn/dt)/n$. At early times when material expands from high densities, the expansion time scale is rather small $\tau_n \approx 1$ ms and the second term in the bracket dominates and consequently the temperature decreases as the material expands. However, as the expansion proceeds and the temperature decreases there will be a moment at which both terms on the right hand side become of the same magnitude. This will correspond to a minimum in the temperature that can be estimated assuming an equation of state dominated by nuclei (Boltzmann ideal gas) and radiation (photons). In this case, we have

$$\varepsilon = \frac{3}{2}\frac{kT}{A} + \frac{aT^4}{n} \quad (3a)$$

$$P = \frac{nkT}{A} + \frac{1}{3}aT^4 \quad (3b)$$

At initial times the average mass number A is about 1, and it grows as the r-process proceeds. Substituting in equation (2) we have:

$$\frac{dT}{dt} = \frac{1}{c_V}\left[\dot{q} - \frac{1}{\tau_n}\left(\frac{4aT^4}{3n} + \frac{kT}{A}\right)\right] \quad (4)$$

The minimum of temperature is reached when the right hand side of the above equation is zero. Initially, when the density is relatively high, the second term in the inner parentheses dominates and we have:

$$T_{\rm min} = 0.05 \text{ GK}\left(\frac{\dot{q}}{4 \text{ MeV s}^{-1}}\right)\left(\frac{\tau_n}{1 \text{ ms}}\right)\left(\frac{A}{1}\right) \quad (5)$$

for the minimal temperature assuming typical values for the other quantities. We see that the minimum temperature is proportional to the expansion timescale. This fact can be understood by noticing that during the expansion the energy generation can only contribute efficiently to increase the temperature during a period of time τ_n. Once the minimum value is reached the temperature starts to rise favored by the fact that the timescale for the expansion grows. However, as the temperature increases and the density decreases the second term in the inner brackets of equation (4) increases. A maximum in temperature is reached once the equation of state becomes dominated by radiation corresponding to a temperature of

$$T_{\rm max} = \left(\frac{3n\dot{q}\tau_n}{4a}\right)^{1/4} \quad (6)$$

$$= 0.8 \text{ GK}\left[\left(\frac{\rho}{10^5 \text{ g cm}^{-3}}\right)\left(\frac{\dot{q}}{4 \text{ MeV s}^{-1}}\right)\left(\frac{\tau_n}{10 \text{ ms}}\right)\right]^{1/4},$$

where we have used typical values for the density, energy generation and expansion timescale. The above discussion clearly shows that the behavior of temperature is determined by basic thermodynamics and it is driven by the fact that at high densities the EoS is dominated by the ideal gas component while at low densities radiation dominates. The dominance of radiation implies a rather large specific heat $c_V \approx 4aT^3/n$ that reduces the efficiency at which the energy generation can contribute to temperature increase. This means that the maxima in temperature is rather flat as observed in the simulations and depends on the expansion timescale at times 0.1 s $\lesssim t \lesssim$ 1 s.

Depending on the trajectories, neutrons are exhausted after 1-2 seconds. Relatedly the r-process comes to an

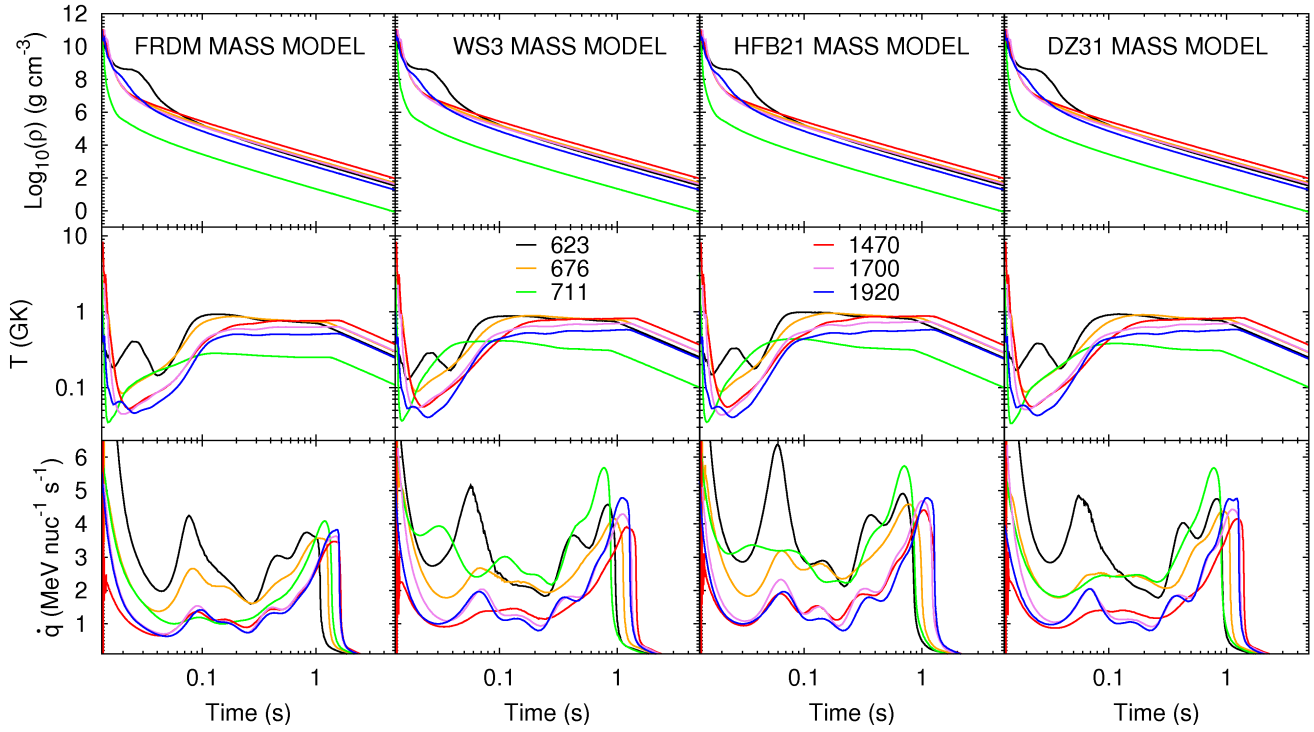

FIG. 1. Evolution of the different thermodynamical variables for the different trajectories, labeled by the initial neutron-to-seed ratio, and mass models used. The upper panels show the evolution of density that is identical for all cases. The middle panel shows the evolution of temperature that considers the feedback due to the energy generation shown in the lower panel.

end with matter decaying back to stability. At this point the energy release due to nuclear reactions drops and the temperature follows an adiabatic expansion that for the radiation dominated conditions implies $T \sim \rho^{1/3}$. It is important to note that the temperature of nearly 10^9 K, which are achieved during most of the r-process due to nuclear reheating, is sufficient to establish an $(n,\gamma) \rightleftarrows (\gamma,n)$ equilibrium for most of the trajectories shown in Figure 1.

There a peculiarities among the trajectories. Some of them develop a 'plateau' in their density profile (example is the trajectory labeled by $R_{n/s} = 623$ in Fig. 1), following the initial period of decompression. During this plateau phase, τ_n is large and the released energy is completely used to heat the system. The temperature profile shows a peak once radiation dominates. After that the expansion accelerates again, followed by a cooling phase before the matter heats again once the expansion rate is reduced. Another trajectory, identified by $R_{n/s} = 711$ in Fig. 1, expands faster than the others. This is connected with a faster drop of the temperature and a lower value of $T_{\rm min}$ related to the smaller τ_n.

The energy release shows quite distint peak structures as function of time. These differences are substantial as a function of mass model. However, they lead to only minor differences in the evolution of temperature as discussed above. The peaks are related to matter being accumulated and then breaking through the r-process waiting points at the magic neutron numbers, where fission cycling, which we will quantify below, induces repetitions of these processes.

The most important observation from Fig. 1, and the arguments given above, is that the temperature during the r-process can be increased to values of a few 10^8 K up to 10^9 K due to reheating by nuclear reactions. Under such high temperatures the r-process resembles the so-called 'hot' r-process scenario rather than a 'cold' r-process as has been commonly assumed in the NS merger context. In a hot r-process, an $(n,\gamma) \rightleftarrows (\gamma,n)$ equilibrium is established and the process evolution and results are usually quite sensitive to masses, while in the cold scenario the r-process proceeds by a competition between neutron capture rates and beta-decays already before freeze out [55].

B. Evolution of the r-process abundances

We have studied r-process nucleosynthesis for the selected set of NS merger trajectories and for the 5 different mass models. The calculated r-process abundances show quite similar general patterns for all mass models which we show in Fig. 2. (The results of DZ10 are not shown as they are almost identical to those of DZ31.) To illustrate special features of r-process nucleosynthesis in NS mergers we show the abundances at 3 different phases of

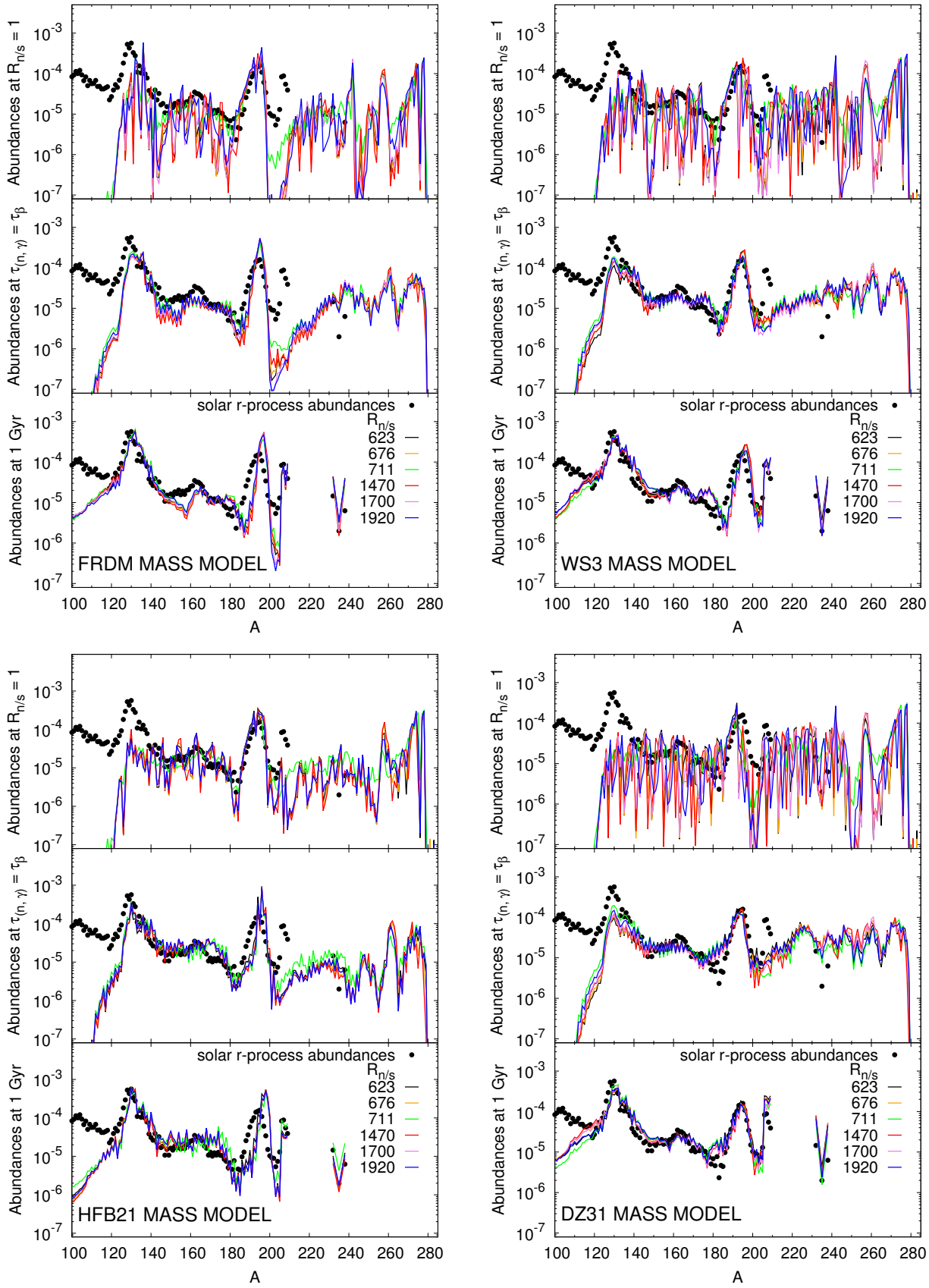

FIG. 2. R-process abundances for the different mass models and trajectories at different phases of the evolution. The upper panels show the abundances at $R_{n/s} = 1$. The middle panel at the time where the average timescales for beta-decay and neutron captures become identical. The lower panel shows the abundances at 1 Gyr when most of the material has already decayed to the stability.

the evolution: a) at freeze out, which we define as the moment where $R_{n/s} = 1$, b) the moment when the average timescale for β decays becomes equal to the average timescale for neutron captures, c) the final abundance, calculated at a time of 1 Gyr.

Comparing the abundances at these 3 different phases we observe the following important features, which are typical of r-process nucleosynthesis in NS mergers. At freeze-out, except for the trajectory that follows a cold r-process, the abundances show a strong odd-even staggering which is washed out subsequently by continuing neutron captures and β decays towards stability. Strikingly, there is no abundance peak at $A \sim 130$, in contrast to the third peak at $A \sim 195$ (the narrow peak at around 138 is seen only in FRDM and will be discussed below). In contrast, the matter flow through the second peak is faster than through the third peak. The origin of this difference is that even at the same neutron separation energy, Q_β values are larger at the $N = 82$ nuclei on the r-process path than for the $N = 126$ nuclei making the respective half-lives significantly shorter. The second abundance peak is produced mainly by fission yields from heavy nuclei around $A \sim 280$ associated with the magic neutron number $N = 184$. At freeze-out, however, there is still a sufficient reservoir of free neutrons from fission and subsequent β decay and photodissociation to support further neutron captures, also on nuclei around $A \sim 130$. These neutron captures (note that $\tau_\beta > \tau_{n,\gamma}$ at freeze out) shape the abundances after freeze out significantly as can be seen when comparing the upper and middle panels in Fig. 2. Importantly, we observe that the second peak now forms (as transport from the fission yields to heavier nuclei by neutron captures is reduced). Furthermore, the strong abundance hole just above $A \sim 195$ is filling up due to decays of heavier nuclei (mainly α decays of nuclei between lead and thorium). Once neutron captures are slower than β decays, matter decays to stability. In particular, the significant amount of matter above lead, still existing in the middle panel, decays to finally form the lead peak. At 1 Gyr only the long-lived thorium and uranium isotopes survive. When comparing the time evolution of the third peak (from the upper to the middle to the lower panel) one clearly notices a shift of the third peak to slightly larger mass numbers in the FRDM mass model. This is caused by neutron captures after freeze-out and confirms the findings reported in [20]. Looking at the final abundances computed for the mass models used in the present study (see Fig. 4) we observe that the shift in the third r-process peak is present in the FRDM and HFB21 mass model but absent in the WS3 and DZ mass models. To understand the reason for this behavior it is important to qualitatively quantify which regions of the nuclear chart are expected to be more relevant for the evolution of the r-process under very general assumptions.

The r-process operates along a path of almost constant neutron separation energy. The speed at which the r-process proceeds from lighter nuclei to heavier nuclei depends on the beta-decay half-lives. Due to the increase in Coulomb energy the valley of stability moves to more neutron rich nuclei with increasing charge number. This means that for a line of constant neutron separation energy the beta-decay Q-values reduce with increasing charge. As a consequence, the beta-decay half-lives of r-process nuclei increase with increasing mass number. On top of this global behavior, there are local effects induced by the presence of neutron shell closures. In particular, at neutron magic numbers $N = 82$ and $N = 126$ the r-process moves closer to stability to nuclei with longer beta-decay half-lives. In the r-process path nuclei with $N \gtrsim 82$ and $N \gtrsim 126$ have the longest half-lives. At freeze-out, it corresponds to charge numbers $Z \approx 48$ and $Z \approx 70$, respectively. The predicted half-lives of these nuclei [26] are of the order of 100 ms which is not much less than the total duration of the r-process, around 1 s. Changing, the time the r-process expends in this long-lived nuclei affects the whole dynamics of the r-process and consequently impacts the r-process abundances. As most of the relevant half-lives are not yet known experimentally the r-process abundances are rather sensitive to the theoretical approach used [23, 56] in computing the half-lives. Alternatively, the effective r-process timescale in the region can change if the r-process path changes due to modifications of the underlying mass model. This is the aspect explored in this work.

Different mass models differ substantially in their predictions in regions where there is a sudden change in the intrinsic deformation [55]. This is particularly the case around $N \sim 90$ and $N \sim 130$ where all mass models used in the present work predict a transition from spherical to deformed configurations. The particular relevance for the r-process is the fact that this transition can be associated with a sudden drop in the neutron separations energies. This is the case for the FRDM mass model as was already pointed out in Ref. [57] for the Tellurium isotopes reaching ^{139}Te. Recent mass measurements for Tellurium isotopes [58, 59] have ruled out this sudden drop in neutron separation energies. However, at present there is no data for lighter isotopes in the region where FRDM also predicts very low neutron separation energies [55]. None of the other models used in the present study show such a drastic reduction in neutron separation energies around $N = 90$. The most noticeable consequence is the presence of a narrow peak around $A \sim 138$ at freeze-out (see upper panel for FRDM mass model in Fig. 2). Due to the accumulation of material in this region, the r-process lasts slightly longer using the FRDM mass model when compared with the other models (see Fig. 1 where the end of the r-process is associated to the drop in the heating rate). The peak becomes washed out at later times due to continuous production of material in this region by fission. However, neutron captures on the fission yields are responsible for a flow of matter from the second r-process peak to heavier nuclei. This flow operates in all used mass models except in FRDM due to the fact that material is halted at $N \sim 90$.

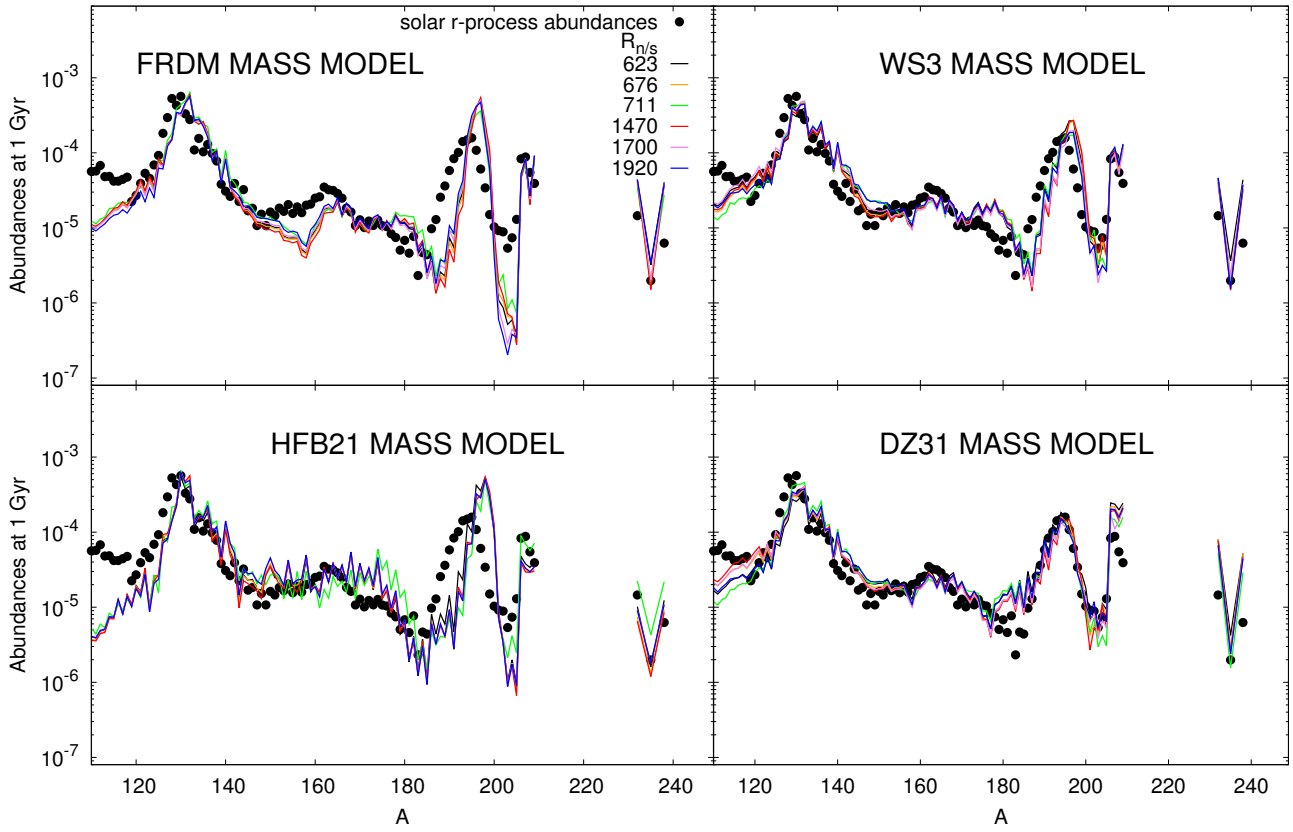

FIG. 3. Final r-process abundances at a time of 1 Gyr for the different mass models and trajectories used in the calculations.

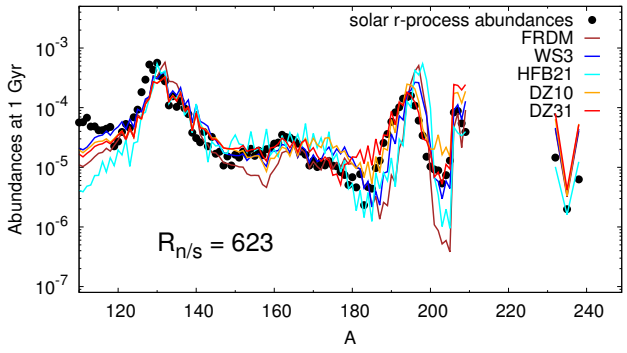

FIG. 4. Final abundances at a time of 1 Gyr for all mass models considered in this work based on the trajectory with initial neutron-to-seed, $R_{n/s} = 623$.

The situation at the third peak is different as the fission yields adopted here do not directly produce material in this region. The third peak abundance is noticeable more sensitive to nuclear masses that influence the neutron capture rates. It is not surprising that the abundances of this peak show a larger variation. However, for two of the mass models (FRDM, HFB21) the peak width is noticeably narrower than observed, the peak height is overestimated, the position shifted slightly to larger mass numbers and an abundance trough is predicted just above the peak. This is related to different behavior of these two models at the neutron number $N = 130$, just above the magic number $N = 126$. The FRDM and HFB21 mass models predict noticeably smaller neutron separation energies than the Duflo-Zuker or the WS3 models in this mass range. For example the nuclei ^{199}Yb, ^{198}Tm and ^{197}Er (all with $N = 129$) have neutron separation energies of $S_n = 0.52$ (0.85) MeV, 0.62 (0.73) MeV, and 0.26 (0.56) MeV, in the FRDM (HFB21) mass models [60], respectively, while they are 1.387 (1.463) MeV, 1.479 (1.528) MeV, and 0.908 (0.864) MeV for the same nuclei in the DZ31 (WS3) models. Thus these nuclei act as (additional) obstacles in r-process simulations using the FRDM and HFB21 mass models, even if the mass flow has overcome the $N = 126$ waiting points. As a result, the third peak in the abundance distribution is shifted for these two mass models to higher mass numbers as can be seen in Fig. 2 caused mainly by late-time neutron captures. Due to the larger neutron separation energies, the $N = 130$ nuclei do not act as obstacles in simulations adopting the Duflo-Zuker or WS3 mass models. Relatedly the third peak develops at $A \sim 195$, associated with the $N = 126$ waiting points.

C. Robust r-process abundances

The final abundances at times of 1 Gyr are shown in Fig. 3. The most striking feature is the fact that the final abundances for mass numbers $A > 130$ are virtually identical for a given mass model for all trajectories. This is similar to the results obtained in refs. [12–14].

Thanks to the large neutron-to-seed ratio found in NS merger conditions the r-process runs through 2–4 fission cycles, where trajectories with larger initial neutron-to-seed ratio obviously support more cycles. This so-called fission cycling has been suggested to be responsible of producing r-process abundances that are almost independent of the astrophysical conditions. Ref. [61] has suggested that fission cycling contributes to produce a steady β flow equilibrium in which the abundances for each isotopic chain are proportional to the beta-decay half-lives. Steady β flow equilibrium is in fact achieved in NS merger before the r-process freeze-out as the duration of the r-process is longer than the individual beta-decay half-lives. Furthermore, it can be achieved both for hot and cold r-process conditions [55]. The upper panels of Fig. 2 show substantial differences in the r-process abundances for the different trajectories that nevertheless converge to a robust abundance pattern at the end of the calculations. This suggest that the mechanism responsible for producing a robust r-process pattern operates after r-process freeze-out and it is independent of the number of fission cycles.

We find that the main requirement to achieve a robust r-process pattern is that the amount of material accumulated at freeze-out in the fissioning region, $A \gtrsim 240$ is much larger than the one present in the region below the 3rd r-process peak. This is guaranteed by the fact that the beta-decay half-lives grow with increasing mass number and by the presence of a neutron shell closure around $N = 184$. Both effects are responsible of producing a peak in the freeze-out r-process abundances around $A \sim 280$ (see upper panels Fig. 2). The material in this peak decays by fission populating mainly the region around the 2nd r-process peak and producing a final robust r-process pattern. Importantly, the general features of this pattern is also independent of the mass models as it is mainly determined by fission yields. This is demonstrated in Figs. 3 and 4 where we compare the final abundances (at 1 Gyr) for four different mass models (FRDM, WS3, HFB21, DZ31) and all trajectories considered in our study and for all mass models and a selected trajectory. Although there are specific differences originating in the dependence of neutron captures on the underlying mass model, all the calculations reproduce the second and third r-process peaks reasonably well. We mention again that the peaks have different origins in our simulations: the peak around $A \sim 130$ arises from fission yields, while the peak at $A \sim 195$ reflects the $N = 126$ waiting points in the matter flow towards heavy nuclei. It is also satisfying to observe that the lead peak around $A \sim 208$ agrees reasonably well with the solar abundances. This peak is mainly produced by α decay of heavier nuclei. Finally also the abundances of the long-lived isotopes ^{232}Th and ^{238}U, which are the final product of some matter with charge numbers $Z \approx 90 - 96$, is reproduced reasonably well.

In details, there are shortcomings of our various calculations when compared to the solar abundances. While the height and the width of the $A \sim 130$ peak is well described by all models, the peak position - mainly due to late-time neutron captures - are slightly shifted to larger mass numbers than observed. The similarity of all models in the description of this peak is related to the fact that we use the same fission yield distributions in all studies. Furthermore our description is noticeable improved compared with those of Refs. [12–14] which might point to an improved description of the fission yields by the ABLA code than by the rather schematic models adopted in previous works [12–14]. Goriely *et al.* [62] have recently presented a new fission fragment distribution that predicts substantial different fission yields for r-process nuclei to those used in the present work. Giving the important role that fission yields play in determining the r-process abundances, it is rather important to further explore the sensitivity of r-process abundances to the fission yields and explore experimental possibilities to constrain them. This goes beyond the goals of the present work.

Finally we mention that, for a given mass model, there are variation in abundances between the different trajectories, which, however, are smaller than between the different mass models. Nevertheless these variations make it impossible to use our calculated U/Th ratios as a cosmochronometer basis to determine the age of metal-poor stars from the observed U/Th ratios. This exercise has to wait for a more complete study of r-process nucleosynthesis in neutron star mergers summing the ejected mass over a large number of trajectories properly weighted with the individual mass ejected by this trajectory as done in Ref. [14].

D. Implications for kilonova observations

One of the most interesting consequences of r-process nucleosynthesis in neutron star mergers is that the large amount of material ejected (around 0.01 $M_\odot$) can produce an electromagnetic transient powered by the radioactive decay of r-process nuclei [12, 14, 53, 63–65]. This transient is commonly denoted as kilonova and may have been recently observed associated with the short γ-ray burst GRB130603B [66, 67].

Modeling kilonova light curves requires the knowledge of the r-process heating rates at timescales between hours and weeks and identify those nuclei that predominantly contribute to the heating rate. This aspect will be explored in further work. In addition, it is also important to know the optical opacities for r-process material as they determine the timescale for photons to escape from the inner opaque region of the ejecta. It has been sug-

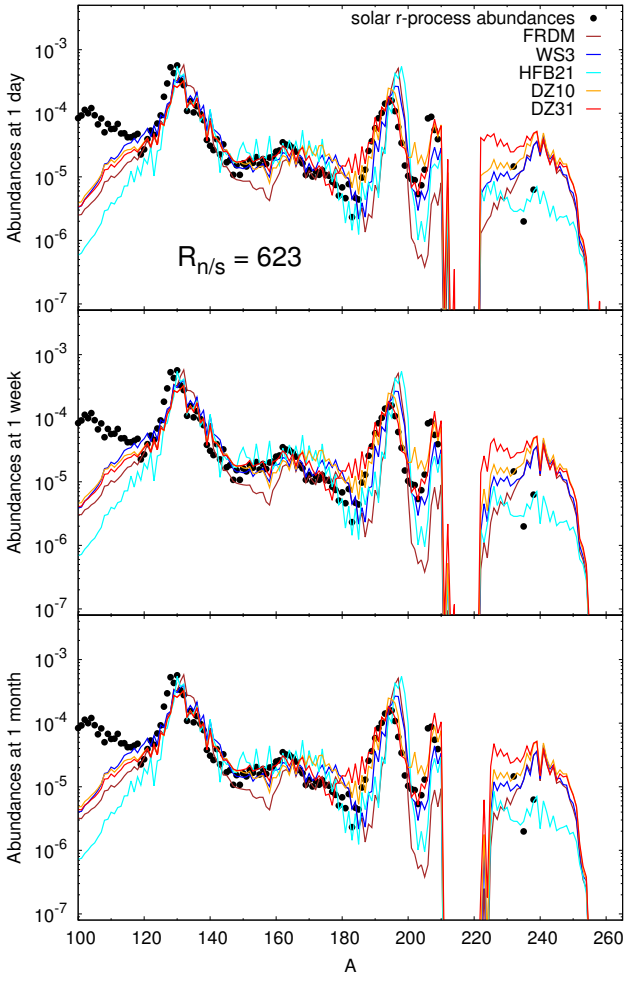

FIG. 5. r-process abundances on timescales relevant for kilonova light curves (upper panel: a day, middle panel: a week, lower panel: a month).

gested that a major source of opacity is due to the presence of lanthanides ($Z = 57$–71, $A \approx 139$–176) [68–70] in the r-process ejecta. Due to their large photon opacities the lanthanides delay the light curve luminosity peak to timescales of a week. The peak frequency is also shifted to the red. An additional source of opacity could be due to the presence of actinides in the r-process ejecta. The r-process in NS mergers ejecta is known to produce the actinides U and Th (see for example Fig. 4). However, at timescales of weeks relevant to kilonova observations the abundance of actinides ($Z = 89$–103, $A \approx 225$–260) can be much larger since many of the nuclei involved have long decay half-lives. This is confirmed in Fig. 5 that shows the r-process abundances at timescales of one day, one week and one month for one of the trajectories considered. As can be seen from Fig. 2, we find a rather small dependence of the actinide abundances on the astrophysical conditions. There is a much larger dependence on the nuclear physics input (see Figs. 2 and 5). This aspect requires further exploration. However, our results demonstrate that the contribution of the actinides to the photon opacities can be substantial.

IV. CONCLUSIONS

In summary, we have performed r-process simulations for various trajectories simulating the spread of conditions obtained in mass ejecta of neutron star merger calculations. Due to the extreme neutron-to-seed ratios achieved, which favor mass transport to the region of fissioning nuclei, fission rates and yields are crucial ingredients in such calculations. Adopting these quantities from the ABLA code which has been adjusted to reproduce fission and fragmentation data and treats the release of neutrons during the fission process explicitly, we have been able to reproduce the main features of the r-process abundances (the second and third peaks, the rare-earth peak and the lead peak) reasonably well. Importantly, we found that these features do not depend sensitively on the astrophysical conditions (but see Ref. [40] for a possible increase of the initial electron fraction which may have an impact on the abundance patterns). We have also shown that these features do not depend in general on the nuclear mass model used. We noticed, however, modest differences in the position of the third peak and in abundance distribution just above this peak around $A \sim 205$. Here the FRDM and HFB21 mass models predict noticeably smaller neutron separation energies for r-process nuclei with $N = 130$ than the other mass models used in our studies. These small separation energies make the $N = 130$ nuclei obstacles in the r-process path resulting in the peak shift and a pronounced abundance trough at $A \sim 205$, if compared to the solar r-process abundances. Experimental work is needed to resolve these different mass predictions for the $N = 130$ nuclei.

Finally, our simulations support the hypothesis that the r-process in dynamical ejecta from neutron star mergers yield rather robust abundance distribution, in good agreement with the observed solar distributions for nuclei with $A \gtrsim 120$. We have shown that a requirement to achieve such a robust pattern is that at freeze-out the amount of material accumulated in the fissioning region ($A \gtrsim 250$) is much larger than the material located in the second r-process peak and above ($A \approx 120$–180). The pile up of material in the fissioning region is guaranteed by the fact that beta-decay half-lives along the r-process path grow with increasing mass number. Nevertheless, it may be sensitive to the detailed shell structure in the region and in particular to the strength of the $N = 184$ shell closure. The decay by fission of this material naturally produces a robust r-process pattern in the region $A \approx$ 120-180 that depends mainly on the used fission yields. Neutron captures during the decay back to stability slightly modify the abundances purely due to fission and are responsible for the small dependence remaining on the astrophysical conditions. The only astrophysical requirement to achieve a robust r-process pattern is that

the neutron to seed ratio is large enough to populate the region of fissioning nuclei. Larger neutron-to-seed ratios increase the amount fission cycles without modifying the final r-process abundance distribution.

We find that for most of the mass models used in the present calculations the amount of actinides present at timescales of several weeks is similar or larger than those of lanthanides. Consequently, actinides may dominate the photon opacities for kilonova light curves.

The NS merger scenario might thus be the one responsible for the robust r-process patterns observed in old metal-poor stars. This requires, however, that the frequency of neutron star mergers is sufficiently large during the early time of our galaxy which is yet an open question.

ACKNOWLEDGMENTS

This work was supported by the Deutsche Forschungsgemeinschaft through contract SFB 634, the Helmholtz International Center for FAIR within the framework of the LOEWE program launched by the state of Hesse, the Helmholtz Association through the Nuclear Astrophysics Virtual Institute (VH-VI-417) and the ExtreMe Matter Institute EMMI in the framework of the Helmholtz Alliance HA216/EMMI. A.B. is a Marie Curie Intra-European Fellow within the 7th European Community Framework Programme (IEF 331873). This work was supported by the Deutsche Forschungsgemeinschaft through Sonderforschungsbereich Transregio 7 "Gravitational Wave Astronomy", and the Cluster of Excellence EXC 153 "Origin and Structure of the Universe".

[1] E. M. Burbidge, G. R. Burbidge, W. A. Fowler, and F. Hoyle, Rev. Mod. Phys. **29**, 547 (1957).
[2] A. G. W. Cameron, *Stellar Evolution, Nuclear Astrophysics, and Nucleogenesis*, Report CRL-41 (Chalk River, 1957).
[3] J. J. Cowan, F.-K. Thielemann, and J. W. Truran, Phys. Repts. **208**, 267 (1991).
[4] M. Arnould, S. Goriely, and K. Takahashi, Phys. Repts. **450**, 97 (2007).
[5] S. E. Woosley, J. R. Wilson, G. J. Mathews, R. D. Hoffman, and B. S. Meyer, Astrophys. J. **433**, 229 (1994).
[6] H.-T. Janka, Ann. Rev. of Nucl. Part. Sci. **62**, 407 (2012).
[7] G. Martínez-Pinedo, T. Fischer, A. Lohs, and L. Huther, Phys. Rev. Lett. **109**, 251104 (2012).
[8] G. Martínez-Pinedo, T. Fischer, and L. Huther, J. Phys. G: Nucl. Part. Phys. **41**, 044008 (2014).
[9] L. F. Roberts, S. Reddy, and G. Shen, Phys. Rev. C **86**, 065803 (2012).
[10] J. M. Lattimer and D. N. Schramm, Astrophys. J. **192**, L145 (1974).
[11] C. Freiburghaus, S. Rosswog, and F.-K. Thielemann, Astrophys. J. **525**, L121 (1999).
[12] S. Goriely, A. Bauswein, and H.-T. Janka, Astrophys. J. **738**, L32 (2011).
[13] O. Korobkin, S. Rosswog, A. Arcones, and C. Winteler, Mon. Not. Roy. Ast. Soc. **426**, 1940 (2012).
[14] A. Bauswein, S. Goriely, and H.-T. Janka, Astrophys. J. **773**, 78 (2013).
[15] C. Sneden, J. J. Cowan, and R. Gallino, Annu. Rev. Astron. Astrophys. **46**, 241 (2008).
[16] R. Fernández and B. D. Metzger, Mon. Not. Roy. Ast. Soc. **435**, 502 (2013).
[17] O. Just, A. Bauswein, R. Ardevol Pulpillo, S. Goriely, and H.-T. Janka, ArXiv e-prints (2014), arXiv:1406.2687 [astro-ph.SR].
[18] B. D. Metzger and R. Fernández, Mon. Not. Roy. Ast. Soc. **441**, 3444 (2014).
[19] A. Perego, S. Rosswog, R. Cabezon, O. Korobkin, R. Kaeppeli, A. Arcones, and M. Liebendoerfer, ArXiv e-prints (2014), arXiv:1405.6730 [astro-ph.HE].
[20] M. Eichler *et al.*, Astrophys. J. (2014), submitted.
[21] J.-J. Gaimard and K.-H. Schmidt, Nucl. Phys. A **531**, 709 (1991).
[22] A. Kelic, M. Valentina Ricciardi, and K.-H. Schmidt, ArXiv e-prints (2009), arXiv:0906.4193 [nucl-th].
[23] L. Caballero *et al.*, Phys. Rev. C (2014), submitted.
[24] I. Borzov, Nucl. Phys. A **777**, 645 (2006).
[25] T. Kurtukian-Nieto, J. Benlliure, K.-H. Schmidt, L. Audouin, F. Becker, B. Blank, I. Borzov, E. Casarejos, F. Farget, M. Fernández-Ordóñez, J. Giovinazzo, D. Henzlova, B. Jurado, K. Langanke, G. Martínez-Pinedo, J. Pereira, and O. Yordanov, Eur. Phys. J. A **50**, 135 (2014).
[26] Q. Zhi, E. Caurier, J. J. Cuenca-García, K. Langanke, G. Martínez-Pinedo, and K. Sieja, Phys. Rev. C **87**, 025803 (2013).
[27] T. Suzuki, T. Yoshida, T. Kajino, and T. Otsuka, Phys. Rev. C **85**, 015802 (2012).
[28] P. Möller, J. R. Nix, W. D. Myers, and W. J. Swiatecki, At. Data Nucl. Data Tables **59**, 185 (1995).
[29] J. M. Pearson, R. C. Nayak, and S. Goriely, Phys. Lett. B **387**, 455 (1996).
[30] M. Liu, N. Wang, Y. Deng, and X. Wu, Phys. Rev. C **84**, 014333 (2011).
[31] J. Duflo and A. P. Zuker, Phys. Rev. C **52**, R23 (1995).
[32] S. Goriely, N. Chamel, and J. M. Pearson, Phys. Rev. Lett. **102**, 152503 (2009).
[33] S. Goriely, N. Chamel, and J. M. Pearson, Phys. Rev. C **82**, 035804 (2010).
[34] R. Oechslin, S. Rosswog, and F.-K. Thielemann, Phys. Rev. D **65**, 103005 (2002).

[35] R. Oechslin, H.-T. Janka, and A. Marek, Astron. & Astrophys. **467**, 395 (2007).

[36] A. Bauswein, H.-T. Janka, and R. Oechslin, Phys. Rev. D **82**, 084043 (2010).

[37] J. Isenberg and J. Nester, in *One hundred years after the birth of Albert Einstein*, General Relativity and Gravitation, Vol. 1, edited by A. Held (Plenum Press, New York, 1980) p. 23.

[38] J. R. Wilson, G. J. Mathews, and P. Marronetti, Phys. Rev. D **54**, 1317 (1996).

[39] M. Ruffert, H.-T. Janka, K. Takahashi, and G. Schaefer, Astron. & Astrophys. **319**, 122 (1997).

[40] S. Wanajo, Y. Sekiguchi, N. Nishimura, K. Kiuchi, K. Kyutoku, and M. Shibata, Astrophys. J. **789**, L39 (2014).

[41] Y. Sugahara and H. Toki, Nucl. Phys. A **579**, 557 (1994).

[42] M. Hempel, T. Fischer, J. Schaffner-Bielich, and M. Liebendörfer, Astrophys. J. **748**, 70 (2012).

[43] A. W. Steiner, M. Hempel, and T. Fischer, Astrophys. J. **774**, 17 (2013).

[44] J. M. Lattimer, Annu. Rev. Nucl. Part. Sci. **62**, 485 (2012).

[45] H. P. Loens, Ph.D. thesis, TU Darmstadt (2010).

[46] P. Möller, B. Pfeiffer, and K.-L. Kratz, Phys. Rev. C **67**, 055802 (2003).

[47] T. Dong and Z. Ren, Eur. Phys. J. A **26**, 69 (2005).

[48] I. V. Panov, I. Y. Korneev, T. Rauscher, G. Martínez-Pinedo, A. Kelić-Heil, N. T. Zinner, and F. Thielemann, Astron. & Astrophys. **513**, A61 (2010).

[49] W. D. Myers and W. J. Świątecki, Phys. Rev. C **60**, 014606 (1999).

[50] I. Petermann, K. Langanke, G. Martínez-Pinedo, I. V. Panov, P.-G. Reinhard, and F.-K. Thielemann, Eur. Phys. J. A **48**, 122 (2012).

[51] N. T. Zinner, Ph.D. thesis, University of Aarhus, Denmark (2007).

[52] B. D. Metzger, A. Arcones, E. Quataert, and G. Martínez-Pinedo, Mon. Not. Roy. Ast. Soc. **402**, 2771 (2010).

[53] B. D. Metzger, G. Martínez-Pinedo, S. Darbha, E. Quataert, A. Arcones, D. Kasen, R. Thomas, P. Nugent, I. V. Panov, and N. T. Zinner, Mon. Not. Roy. Ast. Soc. **406**, 2650 (2010).

[54] F. X. Timmes and D. Arnett, Astrophys. J. Suppl. **125**, 277 (1999).

[55] A. Arcones and G. Martínez-Pinedo, Phys. Rev. C **83**, 045809 (2011).

[56] T. Marketin, L. Huther, and G. Martínez-Pinedo, (2014), in preparation.

[57] B. S. Meyer, G. J. Mathews, W. M. Howard, S. E. Woosley, and R. D. Hoffman, Astrophys. J. **399**, 656 (1992).

[58] J. Hakala, J. Dobaczewski, D. Gorelov, T. Eronen, A. Jokinen, A. Kankainen, V. S. Kolhinen, M. Kortelainen, I. D. Moore, H. Penttilä, S. Rinta-Antila, J. Rissanen, A. Saastamoinen, V. Sonnenschein, and J. Äystö, Phys. Rev. Lett. **109**, 032501 (2012).

[59] J. Van Schelt, D. Lascar, G. Savard, J. A. Clark, S. Caldwell, A. Chaudhuri, J. Fallis, J. P. Greene, A. F. Levand, G. Li, K. S. Sharma, M. G. Sternberg, T. Sun, and B. J. Zabransky, Phys. Rev. C **85**, 045805 (2012).

[60] We note that the low neutron separation energies remain in the latest version of the HFB type mass model, HFB27 [71].

[61] J. Beun, G. C. McLaughlin, R. Surman, and W. R. Hix, Phys. Rev. C **77**, 035804 (2008).

[62] S. Goriely, J.-L. Sida, J.-F. Lemaître, S. Panebianco, N. Dubray, S. Hilaire, A. Bauswein, and H.-T. Janka, Phys. Rev. Lett. **111**, 242502 (2013).

[63] L. Li and B. Paczyński, Astrophys. J. **507**, L59 (1998).

[64] S. R. Kulkarni, ArXiv Astrophysics e-prints (2005), astro-ph/0510256.

[65] L. F. Roberts, D. Kasen, W. H. Lee, and E. Ramirez-Ruiz, Astrophys. J. **736**, L21 (2011).

[66] N. R. Tanvir, A. J. Levan, A. S. Fruchter, J. Hjorth, R. A. Hounsell, K. Wiersema, and R. L. Tunnicliffe, Nature **500**, 547 (2013).

[67] E. Berger, W. Fong, and R. Chornock, Astrophys. J. **774**, L23 (2013).

[68] D. Kasen, N. R. Badnell, and J. Barnes, Astrophys. J. **774**, 25 (2013).

[69] J. Barnes and D. Kasen, Astrophys. J. **775**, 18 (2013).

[70] M. Tanaka and K. Hotokezaka, Astrophys. J. **775**, 113 (2013).

[71] S. Goriely, N. Chamel, and J. M. Pearson, Phys. Rev. C **88**, 061302 (2013).